PCCP

Accepted Manuscript

ROYAL SOCIETY OF CHEMISTRY

www.rsc.org/pccp

PCCP

RSCPublishing

PAPER

Photocatalytic H_2 Evolution on MoS_2/TiO_2 catalysts synthesized via mechanochemistry

Cite this: DOI: 10.1039/xoxxoooooox

Yanyan Zhu[a,b], Qiang Ling[b], Yanfang Liu[a], Hua Wang[b], and Yongfa Zhu[a,*]

Received 00th 2014,
Accepted 00th 2014

DOI: 10.1039/x0xx00000x

www.rsc.org/pccp

Abstract: At present, the composite photocatalysts of MoS_2 cocatalyst and subjective semiconductor material were usually obtained via various complex reduction methods by using NH_4MoS_4 or Na_2MoO_4 as precursor. In this work, a simple method was proposed to synthesize MoS_2/TiO_2 composite photocatalysts via mechanochemistry by using MoS_2 as precusor directly. 4.0% MoS_2/TiO_2 after 300 rpm ball-milling for 2h possessed the maximal photocatalytic activity of H_2 evolution and the rate of H_2 evolution was up to 150.7 μmol·h^{-1}, which was 48.6 times as high as that of pure TiO_2. The MoS_2/TiO_2 had the stable photocatalytic performance of H_2 evolution. Photoelectrochemical measurements confirmed the electronic interaction between TiO_2 and MoS_2. The photo-generated electrons on conduction band of TiO_2 could easily transfer to MoS_2 cocatalyst, which promoted the charges separation efficiently and improved the photocatalytic performance.

1. Introduction

Semiconductor photocatalysis is one of the major methods to solve the energy crisis and environmental pollution. Photocatalytic H_2 evolution from water splitting and CO_2 reduction recently have attracted considerable attentions[1, 2]. Up to now, a series of semiconductor photocatalysts that could be used in the H_2 evolution from water splitting were exploited, such as ultraviolet active TiO_2[3, 4], $SrTiO_3$[5], $In_{1-x}Ni_xTaO_4$[6], visible active C_3N_4[7, 8], Cu_2O[9], CdS[10, 11] and so on. During the process of photocatalytic reaction, cocatalyst can lower the activation potentials for H_2 or O_2 evolution reaction and act as active sites for H_2 or O_2 formation[3]. Moreover, cocatalyst could also enhance photocatalytic performance via the efficient separation of photo-generated charges.

Pt was firstly used as electrocatalyst and cocatalyst of TiO_2, which had positive effect on the H_2 evolution from water splitting[12-16]. Four kinds of cocatalyst materials were studied at present, including noble and coinage metals (Pt, Pd, Ag, Au, Cu, etc.), transition metal oxide (NiO, RuO_2, Mn_2O_3), metal sulfide (MoS_2, WS_2 and PdS) and composite cocatalyst (Ni/NiO, Rh@Cr_2O_3) [1, 17]. However, the use of noble metal for H_2 evolution from water may be difficult in practical application due to its high-cost and scarcity, thus low-cost inorganic materials become the potential and suitable objects. Among the inorganic materials, MoS_2[18-22] as cocatalyst of photocatalyst and CoP, Ni2P, Cu_3P, MoP as electrocatalyst[16, 23-27] was found to be a good candidate to meet the demand of practical application. MoS_2 loading on CdS as cocatalyst exhibited excellently higher photocatalytic H_2 evolution performance than noble metal Pt, Pd and Au[28]. At present, the composite photocatalysts of MoS_2 cocatalyst and subjective semiconductor material were usually obtained via high-temperature calcination in protective gas[19, 22, 28, 29], solvothermal method[18, 20, 21, 30] or photo-deposition[31] technique by using NH_4MoS_4 or Na_2MoO_4 as precursor. The above methods have many shortcomings such as complexity of reaction process, serious secondary pollution, high-cost and incomplete reduction. By comparison, ball-milling as mechanochemistry method is a highly efficient and energy-saving technology for the preparation of composite photocatalyst, which can initiate chemical reaction and induce changes of material structure and performance. This method has obvious advantages such as decreasing the activation energy of reaction, refining crystal particles, enhancing materials activity, improving homogeneity of particles and strengthening the interfacial bonding within different materials. In recent years, many highly active or wide-absorption range composite photocatalysts were synthesized via ball-milling[32-35].

In the present work, MoS_2/TiO_2 composite photocatalysts were synthesized via mechanochemistry by using MoS_2 as precursor directly. The photocatalytic H_2 evolution performances of MoS_2/TiO_2 after different ball-milling speed and various MoS_2 loading amount were investigated. The structure and morphology of MoS_2/TiO_2 were evaluated. The photocatalytic mechanism for the enhanced H_2 evolution activity of MoS_2/TiO_2 was also proposed.

2. Experimental Section

2.1 Chemicals and Reagents

TiO_2 (P25, 20% rutile and 80% anatase) powder was purchased from Degussa Co., Ltd. of Germany. Chemical pure molybdenum disulfide (MoS_2) was purchased from Tianjin No.4 Chemical Reagent Factory of China. Analytic grade Ethanol was purchased from Beijing Chemical Works of China. Chemical pure methanol was purchased from Sinopharm Beijing Chemical Reagent Co., Ltd. All chemical reagents were used directly without any further purification.

2.2 Synthesis of MoS_2/TiO_2 composite photocatalysts

Certain amount of MoS_2 and 2.0 g TiO_2 were mixed in an agate jar, and 4.0 ml of ethanol and agate balls were added subsequently. Then the mixtures were ball-milled at the speed of 300 rpm for 4.0 h and on the XQM-0.4 planetary ball mill, and then the samples were dried in air to remove ethanol completely. The final samples were MoS_2/TiO_2 composite photocatalysts with various MoS_2 loading amount. Moreover, 4.0% MoS_2/TiO_2 photocatalysts at different ball-milling speed were prepared as above method.

2.3 Photocatalytic performance of H_2 evolution

The photocatalytic reactions were carried out in Labsolar-Ⅲ AG photocatalytic on-line analytical system produced by Beijing perfect light technology Co., Ltd. 0.2 g TiO_2 or MoS_2/TiO_2 photocatalysts powder were added into 100 ml 15% methanol-H_2O mixed solution and methanol was used as sacrificial reagent, and the suspensions were ultrasonically dispersed for 10 min. Then the suspension was thoroughly degassed and then irradiated by a 300 W Xe lamp (PLS-SXE300 CUV) equipped with a UV optical filter (250-380 nm). The temperature of the reaction solution was maintained at 5 ± 0.5 ℃ by a flow of cooling liquid during the process of photocatalytic reaction. At each given time intervals, 1.0 mL gas was extracted from sample loop and then analyzed with on-line gas chromatography (GC-7800, molecular sieve 5A column, thermal conductivity detector, N_2 carrier). The total amount of H_2 was calculated using the volume ratio of sample loop and total closed system, and the photocatalytic performances of H_2 evolution were compared by the average rate of H_2 evolution in 6.0 h.

2.4 Materials Characterization

The photocurrents and electrochemical impedance spectroscopy (EIS) were performed on CHI-660B electrochemical system (Shanghai, China) using a platinum wire as counter electrode, a standard calomel electrode (SCE) as reference electrode and a MoS_2/TiO_2 electrodes film on ITO as a working electrode. Photoelectrochemical properties were measured with an 11 W germicidal lamp and 0.1mol·L^{-1} Na_2SO_4 electrolytes were used. The photoelectric responses of the photocatalysts as light on and off were measured at 0.0 V. The electrochemical impedance spectroscopy (EIS) was carried out in the open circuit potential mode, and a sinusoidal ac perturbation of 5 mV was applied to the electrode over the frequency range of 0.05–10^5 Hz. The photoluminescence (PL) emission spectra of TiO_2 and MoS_2/TiO_2 samples were measured on Aqualog®absorbance and 3D fluorescence scanning spectrophotometer equipped with a 150 W xenon lamp with an excitation wavelength of 254 nm.The crystallinity and particle size of as-prepared samples were characterized by a Bruker D8 Advance X-ray diffractometer (Cu Kα=1.5418 Å) at a scan rate of 2°·min^{-1} in the 2θ range from 10° to 60°. The UV–Vis diffuse reflectance spectra (DRS) of the samples were performed on Hitachi U-3010 spectroscope equipped with an integrated sphere attachment in the range of 200 to 800 nm, and $BaSO_4$ was used as a reference sample. The Raman spectrum was measured at room temperature using HORIBAR 800 microscopic confocal Raman spectrometer in the range of 2000 cm^{-1} to 4000 cm^{-1}, and the excitation light was the 514.5 nm from an Ar^+ laser with 30 mW output power. The X-ray photoelectron spectra (XPS) were recorded on an ULVAC-PHI X-ray photoelectron spectrometer (PHI Quantera) using Al Kα radiation, and all binding energies are referred to the C 1s peak of 284.8 eV. The morphologies and structures of the samples were examined with a HITACHI HT7700 transmission electron microscopy (TEM) with an accelerating voltage 100 kV. The high-resolution transmission electron microscopy (HRTEM) images were obtained by JEM2010F transmission electron microscope operated at an accelerating voltage of 200 kV. Results and Discussions

3. Results and dicussion

3.1 Photocatalytic performance and photocurrent of MoS_2/TiO_2

Cocatalyst could efficiently separate and transfer the photo-generated charges and further enhance the photocatalytic activity. Pure MoS_2 had no photocatalytic activity under light irradiation[36]. MoS_2 interacted with TiO_2 on the interface after ball-milling, which could quickly seperate the photo-generated electrons of TiO_2 and improve the photocatalytic activity (Fig.1). The photocatalytic activity of H_2 evolution on pure TiO_2 was very low due to the fast recombination of photo-generated electrons and holes, and the rate of H_2 evolution on TiO_2 was only 3.1 μmol·h^{-1}. With increasing the amount of MoS_2 loading, the rates of H_2 evolution increased remarkably and then decreased gradually, and the results were in accord with literature[22, 37](Fig. 1a). When the amount of MoS_2 loading was 4.0%, MoS_2/TiO_2 photocatalyst reached the maximum rate of photocatalytic H_2 evolution with 150.7 μmol·h^{-1}, which was 48.6 times as high as that of TiO_2. However, when the amount of MoS_2 loading exceeded 4.0%, the photocatalytic H_2 evolution activity of MoS_2/TiO_2 would decrease gradually with the MoS_2 loading amount increasing. Excess black MoS_2 would absorb a lot of light and inhibit the efficient absorption of photons by TiO_2, which may be the reason for the decreased photocatalytic activity. Moreover, the effect of ball-milling speed on the rate of H_2 evolution was also investigated in the scope of 100～350 rpm when MoS_2 loading amount was 4.0%(Fig.1b). Under low ball-milling speed, the rate of H_2 evolution was also low because of the weak interaction between TiO_2 and MoS_2. With the increasing of the ball-milling speed, the rate of H_2 evolution increased further and reached the

maximum value when the ball-milling was 300 rpm. Further increasing the speed of ball-milling to 350 rpm, the rate of H_2 evolution decreased. It is supposed that too quick ball-milling may produce much more defects, which is not conducive to the separation of photo-generated charges. The highest rate of photocatalytic H_2 evolution on MoS_2/CdS obtained by calcining $(NH_4)_2MoS_4$ under H_2S and Ar protective gas was about 22 and 15 times as high as that of pure CdS[22, 28]. The maximum photocatalytic activity of MoS_2/TiO_2 obtained via solvothermal reduction of $(NH_4)_2MoS_4$ was 18.5 times as high as that of pure TiO_2[20]. MoS_2/TiO_2 synthesized via simple wet ball-milling posesse the superior photocatalytic performance on the H_2 evolution from water splitting, which is of great importance to practical application.

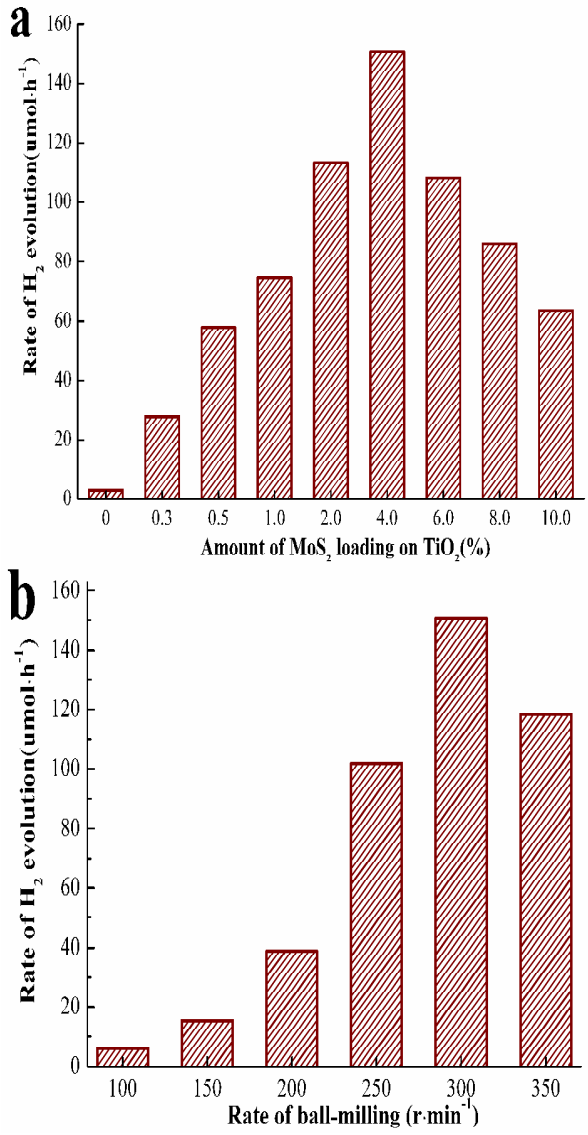

Fig.1 The rate of H_2 evolution on MoS_2/TiO_2 with various MoS_2 loading amount (a) and differernt ball-milling speed (b) in methanol-H_2O mixed solution

In order to evaluate the photocatalytic stability of MoS_2/TiO_2 composites, the 18 h cyclic H_2 evolution experiments for three times every 6 h was performed. As shown in Fig.2, the repetition tests revealed that the amount of H_2 evolution was proportional to reaction time, and the total amounts of H_2 evolution for every times were almost the same. The above results indicated that MoS_2/TiO_2 composite photocatalyst had a good stability in the photocatalytic H_2 evolution reaction process.

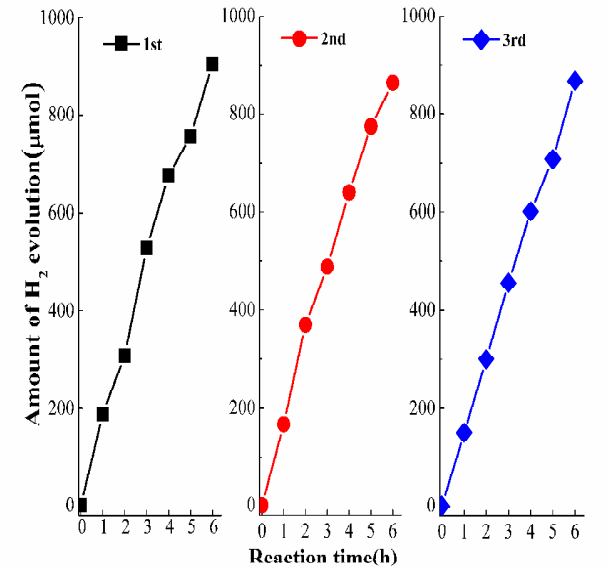

Fig.2 Cyclic H_2 evolution on 4.0% MoS_2/TiO_2 composite photocatalyst for three times

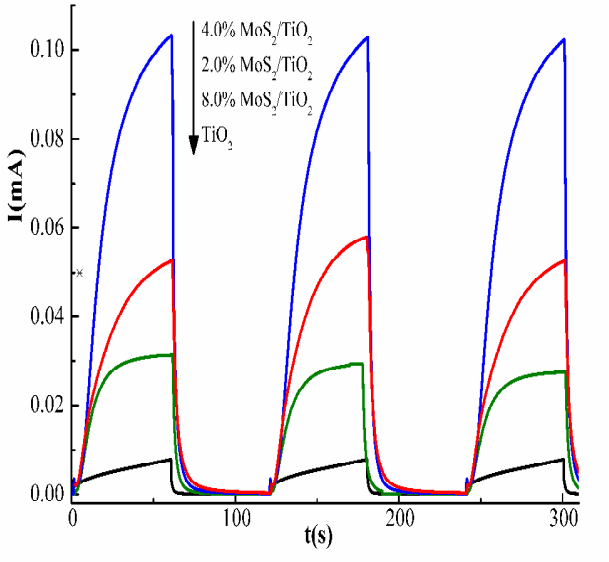

Fig.3 The transient photocurrent responses of TiO_2 and MoS_2/TiO_2 composite photocatalysts electrodes with light-on and light-off cycles

The separation efficiency of photo-generated charges might be correlated with the transient photocurrent responses[38,

[39]. The transient photocurrent responses of pure TiO_2 and MoS_2/TiO_2 with different amount of MoS_2 loading under light irradiation are quite reversible and the electrodes are stable (Fig.3). The photocurrents of MoS_2/TiO_2 photocatalysts were all higher than that of TiO_2. This indicated that MoS_2 cocatalyst enhanced the separation and transfer efficiency of TiO_2 photo-generated charges[19, 20]. At the same time, it was observed that the highest photocurrent of 4.0% MoS_2/TiO_2 was about 0.09 mA and it was 20 times as high as that of TiO_2. This result might be ascribed to the intimate interaction between MoS_2 and TiO_2 interface via ball-milling.

3.2 Structure and morphology of MoS_2/TiO_2

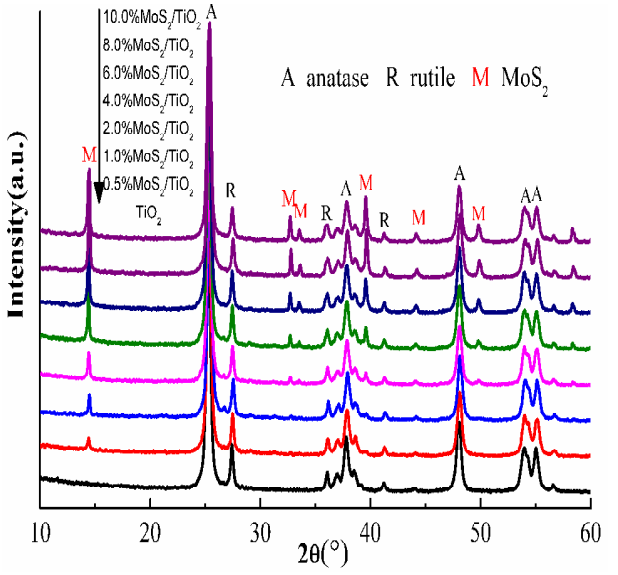

Fig.4 The XRD patterns of TiO_2 and MoS_2/TiO_2 photocatalysts

The phase structures and particle sizes of TiO_2 and MoS_2/TiO_2 samples with different MoS_2 loading amount could be identified by XRD spectra (Fig.4). Pure TiO_2 sample was consisted of anatase and rutile crystal phase. With the MoS_2 loading amount increasing, the characteristic peaks ascribed to (002), (100), (103) and (105) lattice plane of MoS_2 hexagonal molybdenite-2H (JCPDS065-0160) emerged at 14.4°, 32.7°, 39.6° and 49.8° and were strengthened gradually. Because the agate grinding ball and the revolving speed were limited in the process of ball-milling, the grinding materials would have the limited value of particle size. According to the overlaid size calculation of MoS_2 three major (002), (100) and (103) lattice plane from Scherrer equation[32], the particle sizes of MoS_2 were increased gradually with its loading amount increasing (Table.1). When the amount of MoS_2 were 0.5% and 1.0% in MoS_2/TiO_2 sample, the particle sizes of MoS_2 were about 30 nm according to the calculation of the strongest peaks of (002) lattice plane. Upon increasing the MoS_2 amount to 4.0%，the average particle sizes of MoS_2 grew to about 40.0 nm. When the amount MoS_2 loading was increased to 10.0%, the particle sizes of MoS_2 became larger and were about 45.0 nm. The particle size of pure MoS_2 was about 50.0 nm (Fig.S1), which indicated that the MoS_2 became smaller in the particle size and interacted with TiO_2 on the interface during the process of ball-milling.

Table.1 The thickness of MoS_2 major lattice plane in MoS_2/ TiO_2

Lattice plane	（002）	（100）	（103）
0.5%MoS_2/TiO_2	28.8		
1.0% MoS_2/TiO_2	33.7		
2.0% MoS_2/TiO_2	34.7	36.8	35.7
4.0% MoS_2/TiO_2	39.2	40.2	39.4
6.0% MoS_2/TiO_2	38.6	39.4	34.8
8.0% MoS_2/TiO_2	41.0	44.1	43.8
10.0% MoS_2/TiO_2	45.0	43.6	46.2
MoS_2	51.4	52.6	49.6

From the UV-Vis DRS of samples (Fig.5a), it could be seen that the absorption band edge of pure TiO_2 and MoS_2 were about 400 nm and 700 nm respectively, but pure MoS_2 had no photocatalytic performance[36]. With the increasing of MoS_2 loading amount, the absorption intensity of MoS_2/TiO_2 samples in the range of 400～700 nm increased gradually. This was induced by the strong optical absorption of black MoS_2 in visible light region. However, it was also observed that the absorption band edge of MoS_2/TiO_2 shifted about 5 nm to long wavelength compared to pure TiO_2, which illustrated that there were interaction between TiO_2 and MoS_2 on the interface during the process of high energy ball-milling[32, 34, 39].

The characteristic Raman spectra of P25 TiO_2, various MoS_2/TiO_2 and MoS_2 samples were shown in Fig.5b. The characteristic Raman peaks of P25 TiO_2 at 142 cm^{-1}, 197 cm^{-1}, 398 cm^{-1}, 515 cm^{-1} and 640 cm^{-1} were ascribed to the E_{g1}, E_{g2}, B_{1g1}, A_{1g}+B_{1g2} and Eg_3 vibration modes of anatase.[40, 41] The strongest peak at 142 cm^{-1} was the symmetric stretching modes of O-Ti-O. The major Raman peak of rutile was located in 143 cm^{-1}, which was covered by the major peaks of anatase. With the amount of MoS_2 loading increasing in MoS_2/TiO_2, the Raman peaks of TiO_2 at 142 cm^{-1} and 197 cm^{-1} ascribed to E_g vibration mode both were shifted to longer wavenumbers and produced a blue shift. Several groups used phonon confinement models and stoichiometry of TiO_2 to correlate shift and width of the Eg anatase mode at 144 cm^{-1} with the crystalline domain size.[42, 43] According to these reports and blue-shift of E_g mode in MoS_2/TiO_2 compared to TiO_2, the particles of TiO_2 are decreased. However, the peaks at 515, and 640 cm^{-1} were shifted to shorter wavenumbers. These redshifts of Raman peak indicated that intimate interaction existed between MoS_2 and TiO_2. Moreover, the Raman peak at 398 cm^{-1} in TiO_2 was replaced by the two strong peaks of MoS_2 at 378 cm^{-1} and 405 cm^{-1}, which were ascribed to the E_{2g} and A_{1g} vibration modes of MoS_2.[40]

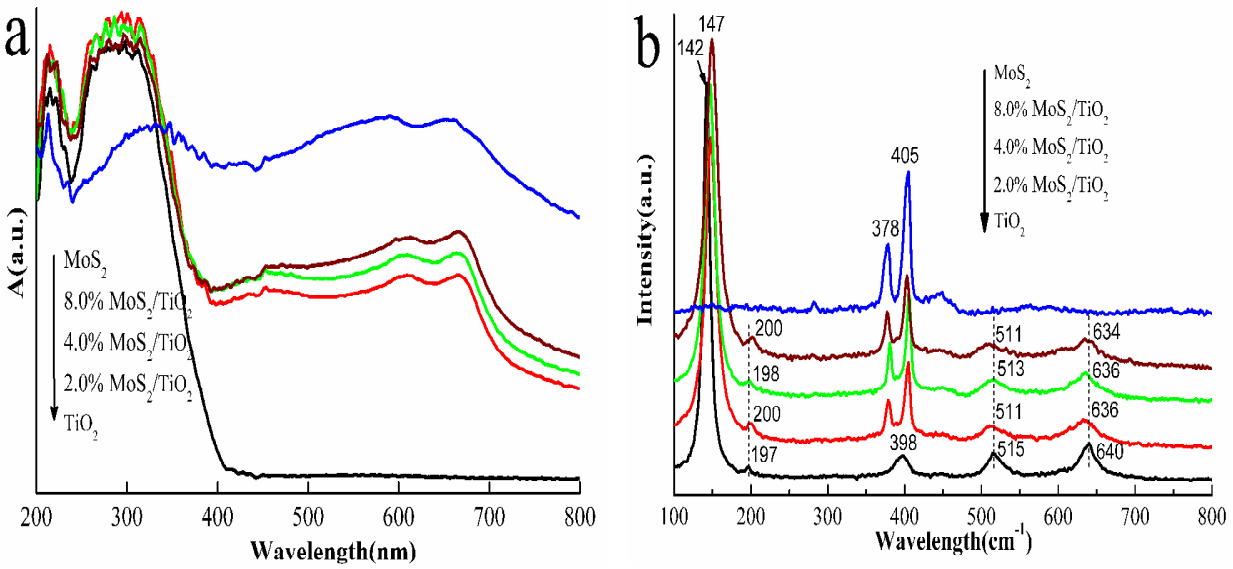

Fig.5 (a) UV–Vis DRS of TiO_2 and MoS_2/TiO_2 photocatalysts with different loading MoS_2 amount; (b) Raman spectra of TiO_2, various MoS_2/TiO_2 and MoS_2 samples

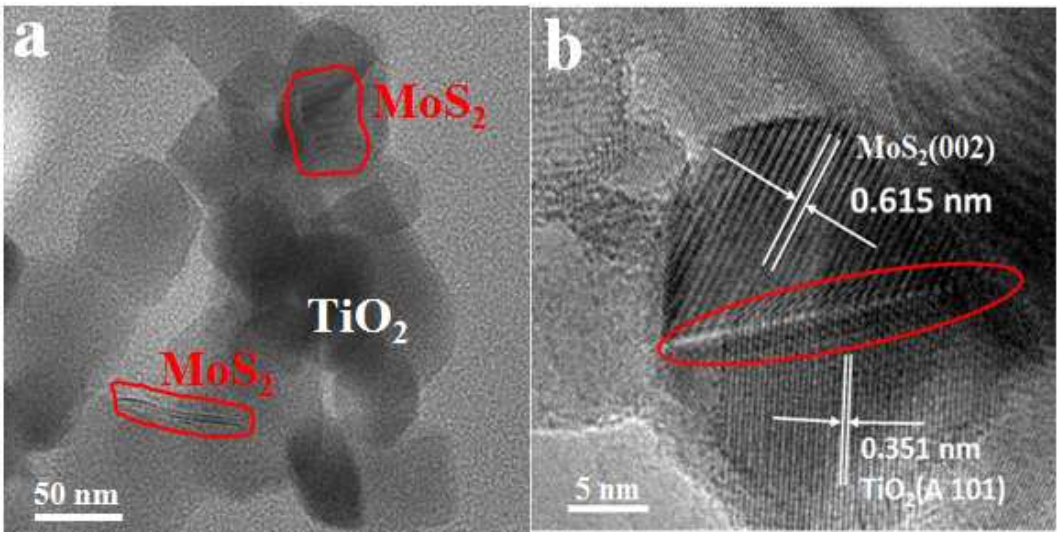

Fig.6 TEM (a) and HRTEM (b) images of 4.0% MoS2/TiO2 photocatalyst

The surface chemical compositions of MoS_2/TiO_2 and chemical states of Ti and Mo in the materials are analysed by XPS (Fig.S2). The binding energies obtained in the XPS analysis were corrected for specimen charging by referencing the C1s line to 284.8 eV. In Fig.S2a, the survey scan XPS spectra provided Ti, O, Mo and S peaks of MoS_2/TiO_2 sample, which were consistent with chemical composition of the Ti^{4+} transfer to the surface of MoS_2 and decrease the electron density of Ti.[45] At the same time, the binding energy of Mo $3d_{5/2}$ and Mo $3d_{3/2}$ produced a largely negative shift compared with pure MoS_2 （Fig.S2c and Fig.S2d）. The shifts of binding energy in MoS_2/TiO_2 indicated the presence of the electron coupling among TiO_2 and MoS_2, which would be beneficial to composite photocatalysts. The binding energy of Ti $2p_{3/2}$ and Ti $2p_{1/2}$ of pure TiO_2 were 458.5 and 464.7 eV respectively, which were consistent with bulk TiO_2.[44] However, the binding energy of Ti $2p_{3/2}$ and Ti $2p_{1/2}$ in MoS_2/TiO_2 composite photocatalysts emerged with 0.2～0.3 eV slightly positive shift(Fig.S2b). Due to the electron-attracting energy of MoS_2, the increase of binding energy on Ti^{4+} might attribute to the electrons around the efficient charges transfer between MoS_2 and TiO_2 during the photocatalytic reaction.

The layered structure of MoS_2 could be found and dispersed in the particles of TiO_2 (Fig.6a and Fig.S3). The particle size of pure TiO_2 was about 50～100 nm in diameter, and that of MoS_2 was 30～50 nm irregular particle consistent with XRD results. From the HRTEM image of 4.0%

MoS_2/TiO_2 (Fig.6b), the lattice fringe with d-spacing of 0.615 nm was in good agreement with (002) lattice plane of MoS_2 （JCPDS 65-0160），and the lattice fringe with d-spacing of 0.351 nm was ascribed to (101) lattice plane of anatase TiO_2 (JCPDS 86-1157). The intimate interaction between MoS_2 and TiO_2 interfaces effectively enhanced the separation and transfer efficiency of photo-generated electrons and further improved photocatalytic performance[29].

3.3 Enhancement Mechanism of MoS_2/TiO_2 Photocatalytic Activity

The arc radius on the EIS spectra reflects the solid state interface layered resistance and the surface charges transfer resistance. The smallest arc radius on the EIS Nyquist plot indicates an efficient separation of the photo-generated electrons and holes, and vice versa[38, 46, 47]. The Nyquist radii of MoS_2/TiO_2 were all smaller than that of TiO_2 in dark and under UV light irradiation (Fig.7), which may be attributed to two reasons: the reduction of surface resistance and the improvement of photo-generated charges separation efficiency induced by high conductivity of MoS_2. As can be seen, 4.0% MoS_2/TiO_2 presented the smallest surface resistance, which was in agreement with its optimal H_2 evolution performance. These results indicated that the MoS_2/TiO_2 composite photocatalysts can promote the migration of photo-generated electrons and decrease the surface resistance, and then further improve H_2 evolution kinetics compared to pure TiO_2.

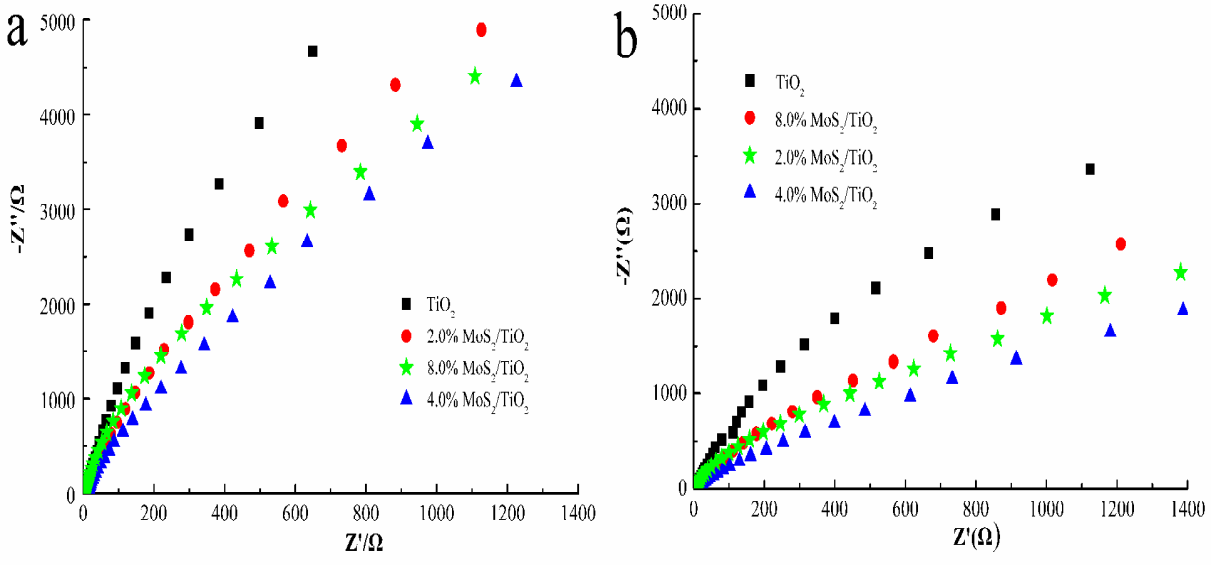

Fig.7 EIS responses of TiO2 and MoS2/TiO2 thin films electrode in dark (a) and under UV irradiation (b)

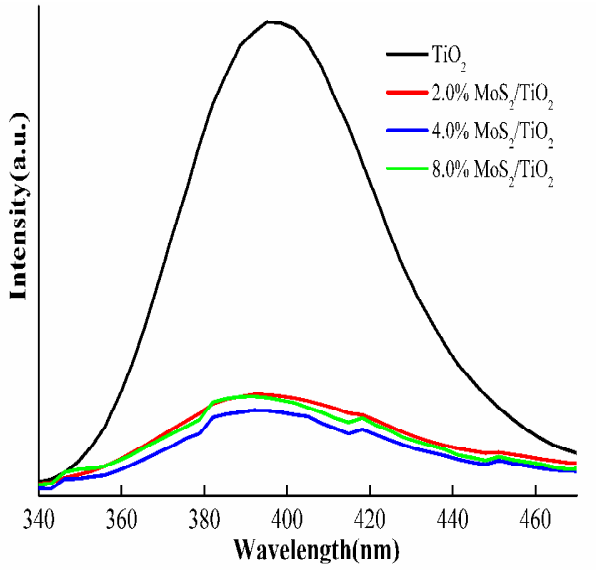

Fig.8 Photoluminescence spectra o TiO2 and MoS2/ TiO2 photocatalysts (λex=254nm).

To some extent, photoluminescence spectra of photocatalyst could reflect the recombination probability of photo-generated electrons and holes.[19, 33, 35] The photoluminescence spectra of TiO_2 and MoS_2/TiO_2 excited at 254 nm were presented (Fig.8). Remarkably, the emission peak of TiO_2 at about 395 nm was quenched in intensity in the presence of MoS_2. This result was attributed to the efficient interfacial electron transfer between MoS_2 and TiO_2, and MoS_2 cocatalyst acted as electron sinks and suppressed the recombination of photo-generated charges[48]. The result corresponds to an efficient charge separation in the MoS_2/TiO_2, which improved the photoelectric and photocatalytic properties of the samples.

The proposed photocatalytic H_2 evolution and charge transfer mechanisms in MoS_2/TiO_2 composite photocatalysts are shown in Fig.9. Under light irradiation, TiO_2 absorbed the photons and generated electron-hole pairs. Photo-generated electrons and holes within the TiO_2 particles either take part in redox reactions on the surface or recombine. The recombination process has a faster kinetics than the redox reactions and

therefore controls the efficiency of the photocatalytic process[43]. On the whole, photo-generated electrons and holes are easy to recombine in pure TiO_2 without cocatalyst loading, which resulted in the low photocatalytic performance. The MoS_2 nanosheets can accept the electrons and act as active sites for H_2 evolution due to its quantum-confinement effect.[40, 41] In the presence of MoS_2, the photo-generated electrons in the conduction band of TiO_2 could be easily transferred to the surface of MoS_2 because of the intimate contact of them. Thus, the possibility of the recombination of e^-/h^+ pairs decrease greatly. The photo-generated electrons on the surface of MoS_2 would react with the adsorbed H^+ ions to form H_2 efficiently.

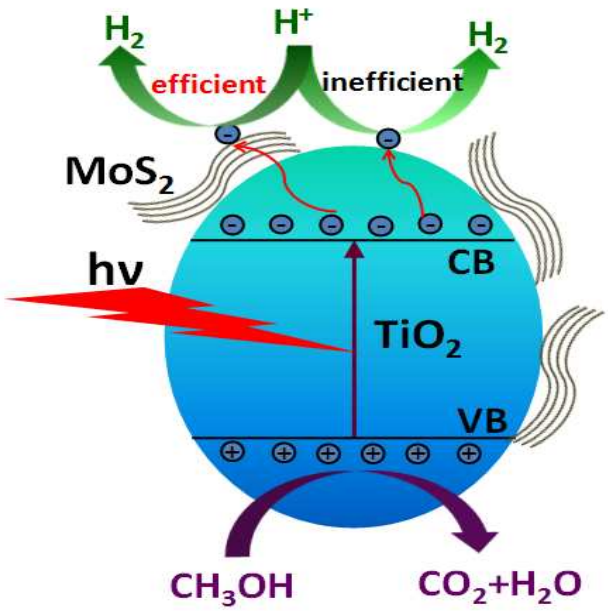

Fig.9 Proposed photocatalytic H_2 evolution and charges transfer mechanism in the MoS_2/TiO_2 composite photocatalyst

4. Conclusions

In conclusion, a simple method was proposed to synthesize MoS_2/TiO_2 composite photocatalyst via mechanochemistry by using MoS_2 as precusor directly. The photocatalytic H_2 evolution performance of MoS_2/TiO_2 was significantly enhanced compared with pure TiO_2, which was ascribed to the intimate interaction between MoS_2 and TiO_2 and the superior conductivity of MoS_2. The 4.0% MoS_2/TiO_2 composite photocatalyst performed the maximal photocatalytic activity of H_2 evolution and its rate of H_2 evolution was up to 150.7 $\mu mol \cdot h^{-1}$, which was 48.6 times as high as that of TiO_2. This work provides a simple, cost-effective and environmental-friendly method to synthesize MoS_2-based composite photocatalysts.

Acknowledgements

This work was partly supported by National Basic Research Program of China (2013CB632403), National High Technology Research and Development Program of China (2012AA062701) and Chinese National Science Foundation (21373121).

Notes

[a] Department of Chemistry, Tsinghua University, Beijing 100084, P.R. China;
b Institute of Aeronautical Meteorology and Chemical Defence, Beijing 100085, P. R. China.

Electronic Supplementary Information (ESI) available: the XRD of MoS_2, TEM images of TiO_2, 2.0% and 4.0% MoS_2/TiO_2. This material is available free of charge by DOI: 10.1039/b000000x/

Corresponding Author

*Fax: (+86)10-6278-7601. Tel.: (+86)10-6278-3586. E-mail: zhuyf@mail.tsinghua.edu.cn.

References

1 W. Fan, Q. Zhang and Y. Wang, *Phys. Chem. Chem. Phys*, 2013, **15**, 2632-2649.
2 S. Protti, A. Albini and N. Serpone, *Phys. Chem. Chem. Phys*, 2014, **16**, 197910-119827.
3 X.-J. Lv, S.-X. Zhou, C. Zhang, H.-X. Chang, Y. Chen and W.-F. Fu, *Journal of Materials Chemistry*, 2012, **22**, 18542-18549.
4 W. Wang, S. Liu, L. Nie, B. Cheng and J. Yu, *Physical Chemistry Chemical Physics*, 2013, **15**, 12033-12039.
5 K. Domen, S. Naito, M. Soma, T. Onishi and K. Tamaru, *Journal Of the Chemical Society-Chemical Communications*, 1980, **12**,543-544.
6 Z. G. Zou, J. H. Ye, K. Sayama and H. Arakawa, *Nature*, 2001, **414**, 625-627.
7 J. Hong, Y. Wang, Y. Wang, W. Zhang and R. Xu, *ChemSusChem*, 2013, **6**, 2263-2268.
8 Y. Sui, J. Liu, Y. Zhang, X. Tian and W. Chen, *Nanoscale*, 2013, **5**, 9150-9155.
9 L. Li, L. Xu, W. Shi and J. Guan, *International Journal of Hydrogen Energy*, 2013, **38**, 816-822.
10 W. Cui, L. Liu, S. Ma, Y. Liang and Z. Zhang, *Catalysis Today*, 2013, **207**, 44-49.
11 W. Cui, Y. Liu, L. Liu, J. Hu and Y. Liang, *Applied Catalysis A: General*, 2012, **417-418**, 111-118.
12 S. Sato and J. M. White, *Chemical Physics Letters*, 1980, **72**, 83-86.
13 S. Sato and J. M. White, *Journal Of Catalysis*, 1981, **69**, 128-139.
14 Z. Xing, Q. Liu, A. M. Asiri and X. Sun, *Advanced materials*, 2014, **26**, 5702-5707.
15 J. Tian, Q. Liu, N. Cheng, A. M. Asiri and X. Sun, *Angewandte Chemie*, 2014, **53**, 9577-9581.
16 E. J. Popczun, C. G. Read, C. W. Roske, N. S. Lewis and R. E. Schaak, *Angewandte Chemie*, 2014, **53**, 5427-5430.
17 F. Wen, J. Yang, X. Zong, Y. Ma, Q. Xu, B. Ma and C. Li, *Progress In Chemistry*, 2009, **21**, 2285-2302.
18 Y. Min, G. He, Q. Xu and Y. Chen, *Journal of Materials Chemistry A*, 2014, **2**, 2578-2584.

19 Y. Liu, Y.-X. Yu and W.-D. Zhang, *Journal Of Physical Chemistry C*, 2013, **117**, 12949-12957.
20 Q. Liu, Z. Pu, A. M. Asiri, A. H. Qusti, A. O. Al-Youbi and X. Sun, *Journal of Nanoparticle Research*, 2013, **15**, 2057-2064.
21 T. Jia, A. Kolpin, C. Ma, R. C. Chan, W. M. Kwok and S. C. Tsang, *Chemical communications*, 2014, **50**, 1185-1188.
22 G. Chen, D. Li, F. Li, Y. Fan, H. Zhao, Y. Luo, R. Yu and Q. Meng, *Applied Catalysis A: General*, 2012, **443-444**, 138-144.
23 J. Tian, Q. Liu, A. M. Asiri and X. Sun, *J Am Chem Soc*, 2014, **136**, 7587-7590.
24 E. J. Popczun, J. R. McKone, C. G. Read, A. J. Biacchi, A. M. Wiltrout, N. S. Lewis and R. E. Schaak, *J Am Chem Soc*, 2013, **135**, 9267-9270.
25 Q. Liu, J. Tian, W. Cui, P. Jiang, N. Cheng, A. M. Asiri and X. Sun, *Angewandte Chemie*, 2014, **53**, 6710-6714.
26 L. Q. Pu Zonghua, Tang Chun , Asiribc Abdullah M.,Sun Xuping *Nanoscale*, 2014, **6**, 11031–11034.
27 Z. Pu, Q. Liu, P. Jiang, A. M. Asiri, A. Y. Obaid and X. Sun, *Chemistry of Materials*, 2014, **26**, 4326-4329.
28 X. Zong, H. Yan, G. Wu, G. Ma, F. Wen, L. Wang and C. Li, *Journal Of the American Chemical Society*, 2008, **130**, 7176-7177.
29 G. W. Xu Zong, Hongjian Yan, Guijun Ma, Jingying Shi, Fuyu Wen, Lu Wang, and C. Li, *J. Phys. Chem. C*, 2010, **114**, 1963-1968.
30 Y. Yan, X. M. Ge, Z. L. Liu, J. Y. Wang, J. M. Lee and X. Wang, *Nanoscale*, 2013, **5**, 7768-7771.
31 S. Kanda, T. Akita, M. Fujishima and H. Tada, *Journal of colloid and interface science*, 2011, **354**, 607-610.
32 C. Shifu, C. Lei, G. Shen and C. Gengyu, *Powder Technology*, 2005, **160**, 198-202.
33 S. Chen, W. Zhao, W. Liu and S. Zhang, *Applied Surface Science*, 2008, **255**, 2478-2484.
34 L. Wei, C. Shifu, Z. Sujuan, Z. Wei, Z. Huaye and Y. Xiaoling, *Journal of Nanoparticle Research*, 2009, **12**, 1355-1366.
35 W. Zhao, Y. Jin, C. H. Gao, W. Gu, Z. M. Jin, Y. L. Lei and L. S. Liao, *Materials Chemistry and Physics*, 2014, **143**, 952-962.
36 A. Sobczynski, *Journal Of Catalysis*, 1991, **131**, 156-166.
37 X. Zong, J. Han, G. Ma, H. Yan, G. Wu and C. Li, *The Journal of Physical Chemistry C*, 2011, **115**, 12202-12208.
38 C. Pan, J. Xu, Y. Wang, D. Li and Y. Zhu, *Advanced Functional Materials*, 2012, **22**, 1518-1524.
39 Y. Wang, R. Shi, J. Lin and Y. Zhu, *Energy Environ. Sci.*, 2011, **4**, 2922-2929.
40 Q. Xiang, J. Yu and M. Jaroniec, *J Am Chem Soc*, 2012, **134**, 6575-6578.
41 K. Zhou, Y. Zhu, X. Yang, X. Jiang and C. Li, *New Journal of Chemistry*, 2011, **35**, 353-359.
42 Y. L. H. W F Zhang, M S Zhang, Z Yin, Q Chen, *J. Phys. D: Appl. Phys.*, 2000, **363**, 912-915.
43 L.-W. Zhang, H.-B. Fu and Y.-F. Zhu, *Advanced Functional Materials*, 2008, **18**, 2180-2189.
44 B. Wang, L. Guo, M. He and T. He, *Phys. Chem. Chem. Phys*, 2013, **15**, 9891-9898.
45 B. Zhu, B. Lin, Y. Zhou, P. Sun, Q. Yao, Y. Chen and B. Gao, *Journal of Materials Chemistry A*, 2014, **2**, 3819.
46 Y. Hou, A. B. Laursen, J. Zhang, G. Zhang, Y. Zhu, X. Wang, S. Dahl and I. Chorkendorff, *Angewandte Chemie*, 2013, **52**, 3621-3625.
47 Y. Lv, Y. Liu, Y. Zhu and Y. Zhu, *Journal of Materials Chemistry A*, 2014, **2**, 1174-1182.
48 X. Bai, R. Zong, C. Li, D. Liu, Y. Liu and Y. Zhu, *Applied Catalysis B: Environmental*, 2014, **147**, 82-91.